

The great 1933 Sanriku-oki earthquake: reappraisal of the main shock and its aftershocks and implications for its tsunami using regional tsunami and seismic data

Naoki Uchida,¹ Stephen H. Kirby,² Norihito Umino,¹ Ryota Hino¹ and Tomoe Kazakami³

¹Research Center for Prediction of Earthquakes and Volcanic Eruptions, Graduate School of Science, Tohoku University, Sendai 980-8578, Japan.

E-mail: naoki.uchida.b6@tohoku.ac.jp

²U.S. Geological Survey, Menlo Park, CA 94025, USA

³National Research Institute for Earth Science and Disaster Prevention, Tsukuba 305-0006, Japan

Accepted 2016 June 20. Received 2016 June 14; in original form 2015 November 6

SUMMARY

The aftershock distribution of the 1933 Sanriku-oki outer trench earthquake is estimated by using modern relocation methods and a newly developed velocity structure to examine the spatial extent of the source-fault and the possibility of a triggered interplate seismicity. In this study, we first examined the regional data quality of the 1933 earthquake based on smoked-paper records and then relocated the earthquakes by using the 3-D velocity structure and double-difference method. The improvements of hypocentre locations using these methods were confirmed by the examination of recent earthquakes that are accurately located based on ocean bottom seismometer data. The results show that the 1933 aftershocks occurred under both the outer- and inner-trench-slope regions. In the outer-trench-slope region, aftershocks are distributed in a ~280-km-long area and their depths are shallower than 50 km. Although we could not constrain the fault geometry from the hypocentre distribution, the depth distribution suggests the whole lithosphere is probably not under deviatoric tension at the time of the 1933 earthquake. The occurrence of aftershocks under the inner trench slope was also confirmed by an investigation of waveform frequency difference between outer and inner trench earthquakes as recorded at Mizusawa. The earthquakes under the inner trench slope were shallow (depth ≤ 30 km) and the waveforms show a low-frequency character similar to the waveforms of recent, precisely located earthquakes in the same area. They are also located where recent activity of interplate thrust earthquakes is high. These suggest that the 1933 outer-trench-slope main shock triggered interplate earthquakes, which is an unusual case in the order of occurrence in contrast with the more common pairing of a large initial interplate shock with subsequent outer-slope earthquakes. The off-trench earthquakes are distributed about 80 km width in the trench perpendicular direction. This wide width cannot be explained from a single high-angle fault confined at a shallow depth (depth ≤ 50 km). The upward motion of the 1933 tsunami waveform records observed at Sanriku coast also cannot be explained from a single high-angle west-dipping normal fault. If we consider additional fault, involvement of high-angle, east-dipping normal faults can better explain the tsunami first motion and triggering of the aftershock in a wide area under the outer trench slope. Therefore multiple off-trench normal faults may have activated during the 1933 earthquake. We also relocated recent (2001–2012) seismicity by the same method. The results show that the present seismicity in the outer-trench-slope region can be divided into several groups along the trench. Comparison of the 1933 rupture dimensions based on our aftershock relocations with the morphologies of fault scarps in the outer trench slope suggest that the rupture was limited to the region

where fault scarps are largely trench parallel and cross cut the seafloor spreading fabric. These findings imply that bending geometry and structural segmentation of the incoming plate largely controls the spatial extent of the 1933 seismogenic faulting. In this shallow rupture model for this largest outer trench earthquake, triggered seismicity in the forearc and structural control of faulting represent an important deformation styles for off-trench and shallow megathrust zones.

Key words: Earthquake dynamics; Earthquake source observations; Seismicity and tectonics; Subduction zone processes; Dynamics: seismotectonics; Pacific Ocean.

1 INTRODUCTION

The 1933 Sanriku-oki earthquake offshore northern Honshu, Japan (M_w 8.4) is the largest earthquake that has recognized to date in the outer-rise/outer-trench-slope regions of the Earth. The ground shaking at Sanriku coast about 300 km to the west of this source was not so large, but the rupture caused a huge tsunami that led to about 3000 deaths (The Central Meteorological Observatory 1933). The maximum tsunami inundation height was 23 m at Ryouri-Shirahama town along the Sanriku coast (Kunitomi 1933; Fig. 1a). The focal mechanism is considered to be a high-angle normal fault based on the first-motion polarity of seismic waveforms and the hypocentral depth is shallow based on its earthquake location (Kanamori 1971; Okal *et al.* 2016).

Outer-rise/outer-trench-slope faulting is considered a pathway for the water supply and hydration into the deep Earth, because such brittle faults provide a means by which seawater may infiltrate into the mantle part of incoming plate and hydrate it (Peacock 2001; Ranero *et al.* 2003; Lefeldt *et al.* 2009). This hydration process is also important for the source process of deep intraplate earthquakes where subsequent dehydration is a plausible cause of the intermediate-depth earthquake occurrence (Kirby *et al.* 1996; Kita *et al.* 2006; Kawakatsu & Watada 2007; Tsuji *et al.* 2008; Nakajima *et al.* 2009) and a water flux that leads to arc magmatism (Iwamori 2000; Hasegawa & Nakajima 2004). Seismic wave speed reduction and inferred weakening of the incoming plate near the trench is evident in tomographic joint inversions of seismic refraction and wide-angle reflection data (Ivandić *et al.* 2008).

The occurrence of outer-rise/outer-trench-slope earthquakes following large interplate earthquakes is well documented for many such earthquakes (Christensen & Ruff 1988; Wartman *et al.* 2009). The M_w 9.0 2011 Tohoku-oki earthquake that occurred in the same subduction zone as the 1933 event was also followed by M_w 7.6 and many other outer-trench-slope earthquakes (Asano *et al.* 2011; Lay *et al.* 2011; Obana *et al.* 2012). Lay *et al.* (2011) argue that the 1933 earthquake followed the 1896 tsunami earthquake that occurred in the adjacent inner trench slope region (Fig. 1a; Tanioka & Satake 1996). However, the reverse case of triggering of interplate earthquakes by outer rise/outer trench slope earthquake is less common. Lay *et al.* (2010) suggest that the 2009 Samoa-Tonga event (M_w 8.1) is also a rare example of an outer trench slope earthquake triggering an interplate faulting subevent (M_w 7.8) that occurred 2 min after the first normal-faulting subevent. However, Beavan *et al.* (2010) suggest for the same earthquake that a slow interplate earthquake occurred first and triggered the outer-trench-slope earthquake. Todd & Lay (2013) showed an example of a large 2011 Kermadec outer-trench-slope intraplate earthquake that triggered interplate earthquakes.

The 3-month aftershock map of the 1933 earthquake from the Japan Meteorological Agency's (JMA)'s standard earthquake location catalogue shows events that are distributed over a wide

area, not only under the outer-trench-slope region but also under the inner-trench-slope region. Thus, it is important to investigate whether these inner-trench-slope aftershocks are due to location errors of their hypocentres or if these events represent seismicity in the megathrust zone that was activated following the 1933 outer-trench-slope normal-faulting earthquake. The recent slip history and mode in this area are also important for understanding the coupling state and stress state of the shallow plate boundary, especially since large interplate thrust slip occurred near the trench during the 2011 Tohoku-oki earthquake (Fujiwara *et al.* 2011; Inuma *et al.* 2011). Such comparisons are also useful for understanding the relationship of the 1933 events to the tsunami earthquake that occurred in 1896 (Tanioka & Satake 1996) in the adjacent forearc.

2 THE SOURCE MODELS OF THE GREAT 1933 SANRIKU-OKI EARTHQUAKE

To model observed long-period surface waves and near-field displacement waveforms, Kanamori (1971) constructed a seismic rupture model as a 185×100 km seismogenic fault dipping 45° towards $N90^\circ W$ (Fig. 1b) that explains the 1933 main-shock waveforms with a uniform slip of 3.3 m. The fault length (185 km) was based on the one-day aftershock distribution and the dip angle was based on a first motion fault plane solution (45°). The 100-km fault width was based on a 70-km horizontal width of the aftershocks and the fault dip angle ($70/\cos 45^\circ \approx 100$ km) suggesting the fault rupture extended to a maximum depth of about 70 km (Fig. 1b). From an estimated thickness of the oceanic lithosphere of 70 km (Kanamori & Press 1970), he concluded that rupture cut through the entire thickness of the Pacific-Plate lithosphere. Although, some recent studies suggest thicker lithosphere for the study region (80–100 km; Zhao *et al.* 1994; Tonegawa *et al.* 2006; Kawakatsu *et al.* 2009), the depth extent of the rupture is still large fraction of the lithosphere thickness. However, observations of focal mechanisms of recent events (2000–2006) near the 1933 earthquake suggest a stress-state reversal from a shallower level (normal faulting at 10–20 km depth) to deeper level (reverse faulting at 25–40 km depth) (Gamage *et al.* 2009). Therefore, a full lithosphere rupture during the 1933 main shock is unlikely to have occurred given the present-day the stress state.

From the point of view of the initial motion of tsunami waves, Abe (1978) noted that the Kanamori's (1971) fault model could not explain the tsunami first motions at the Sanriku coast, to the west of the main-shock epicentre (Fig. 1a)—Kanamori's model predicted a downward first motion, but all of the four Sanriku-coast tide-gauges in the Abe's paper show an upward tsunami first motions. To fit observed tsunami waveforms, Abe proposed the same west-dipping fault but with a smaller dip angle (30°) than the Kanamori's model (45°) (Fig. 1b). Aida (1977) suggests from tsunami wave

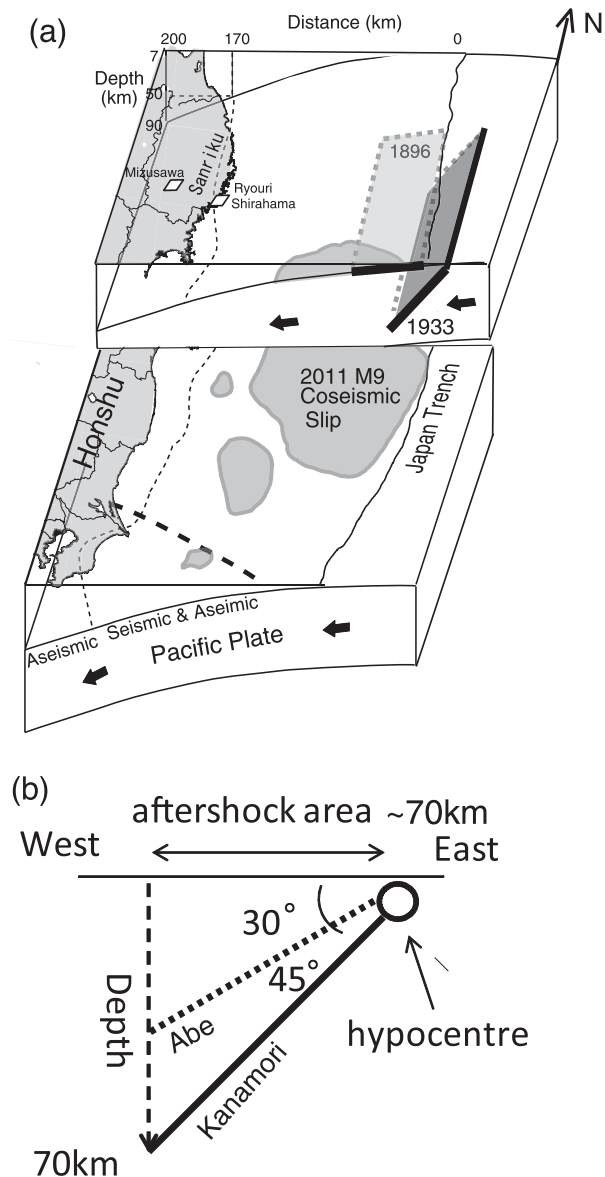


Figure 1. (a) Schematic diagram of the Japan trench subduction system showing the approximate location of the 1933 fault model (Kanamori 1971), the 1896 earthquake fault model (Tanioka & Satake 1996) and the 2011 Tohoku-oki earthquake fault model (Iinuma *et al.* 2012). The location of Ryouri-Shirahama town and Mizusawa latitude observatory are also shown. (b) East-west cross-section showing the Kanamori (1971), Abe (1978) and Okal *et al.* (2016) models for the 1933 rupture.

simulation that a model with half the width of Kanamori (1971) fault model better explains the tsunami waveforms. These fault models do not suggest full-lithosphere rupture and, hence there is a disparity between the Kanamori's rupture model and the tsunami observations.

Although outer-trench-slope seismicity in the source area is dominantly of the normal faulting type (Koyama *et al.* 1973) as expected in a plate bending environment, the existence of deeper reverse fault earthquakes (41 km) was found by (Seno & Gonzalez 1987). Gamage *et al.* (2009) found a shallow double-planned seismic zone with a depth separation of 28–32 km in the forearc region including the region beneath the Japan trench. They showed the upper-plane events are characterized by normal faulting and lower-plane events are characterized by reverse faulting. The 2011 March 11 M_w 9.0

Tohoku-oki interplate earthquake triggered a pulse of outer-rise seismicity after the earthquake (Lay *et al.* 2011; Obana *et al.* 2012). Obana *et al.* (2012) indicate that tensional stresses extended to depths of as much as 40 km after the Tohoku-oki earthquake, significantly deeper than the depth limit of normal faulting earthquake before the earthquake (≈ 20 km). The faulting mechanism of the 1933 event is relevant to the rheological properties of the incoming Pacific plate and the stress state near the plate boundary.

In this study, we relocated the aftershocks of the 1933 earthquake using modern methods, including both a regional velocity structure and a double-difference method (Zhang & Thurber 2003). In addition, we employed new observations of the regional waveform characteristics of aftershocks that occurred in the near-trench region to test the distribution of earthquakes. We interpret these hypocentres as well as the main-shock focal mechanism and tsunami waveforms to discuss the depth extent of the main shock and possibility of the activation of multiple faults during and/or after the 1933 earthquake. We also show that triggering of interplate aftershocks by stress transfer from the 1933 main shock best satisfies the aftershocks under the shallow inner trench slope.

3 DATA AND TEST RELOCATION

We use JMA's phase data for the hypocentre relocations of the 1933 earthquake and its aftershocks. It is important to know accuracy of the data and the stability of the hypocentre location when discussing results from this dataset that has relatively large uncertainties. To estimate the accuracy of the phase data in 1933, we re-picked the earthquake phases by using smoked-paper records obtained at the Mizusawa station where timing was established using on-site astronomical observations at the Mizusawa Astronomical observatory (39.13°N, 141.13°E, about 300 km west of the main shock, Fig. 1). We successfully obtained 27 S - P times (Supporting Information Table S1). The S - P time versus P -origin time plot (called Wadati diagram; (Umino *et al.* 2006)) is shown in Fig. 2 together with that for JMA data and the catalogue of Mizusawa Latitude Observatory (The International Latitude Observatory of Mizusawa 1984). Here, we used JMA origin times from the JMA catalogue. In this figure, the data are supposed to be distributed along a line whose slope is determined from the ratio of P - to S -wave velocity but there are large departures from this line. From visual inspection of the waveforms and the Wadati diagram, we consider there is about a 5 s uncertainty stemming from station clock inaccuracy and the resolution of time on the seismogram as well as drum-speed drift. Next, we performed test hypocentre relocations using several methods to compare the resulting scatter in the locations over characteristics for 3 months after the main shock using a 1-D velocity structure. The JMA catalogue shows an earthquake distribution both to the east and west of the Japan trench and the main-shock hypocentre is located slightly east of the off-trench aftershock distribution (Fig. 3a). When the actual velocity structure varies both with latitude and longitude as well as with depth, and cannot be modelled well by 1-D velocity structure, the use of stations at different ranges from the hypocentre can cause a systematic shift of apparent hypocentre locations. Since the 1933 earthquake is large, there are phase data from distant stations (more than 1500 km away) compared with relatively small aftershocks recorded only at regional stations. Therefore we relocated the earthquakes by restricting the phase data to regional distances (squares in Fig. 3b) to obtain better-resolved relative locations for the aftershocks and main shock. Relocation by using the routine Tohoku university's procedure (Hasegawa *et al.* 1978) using

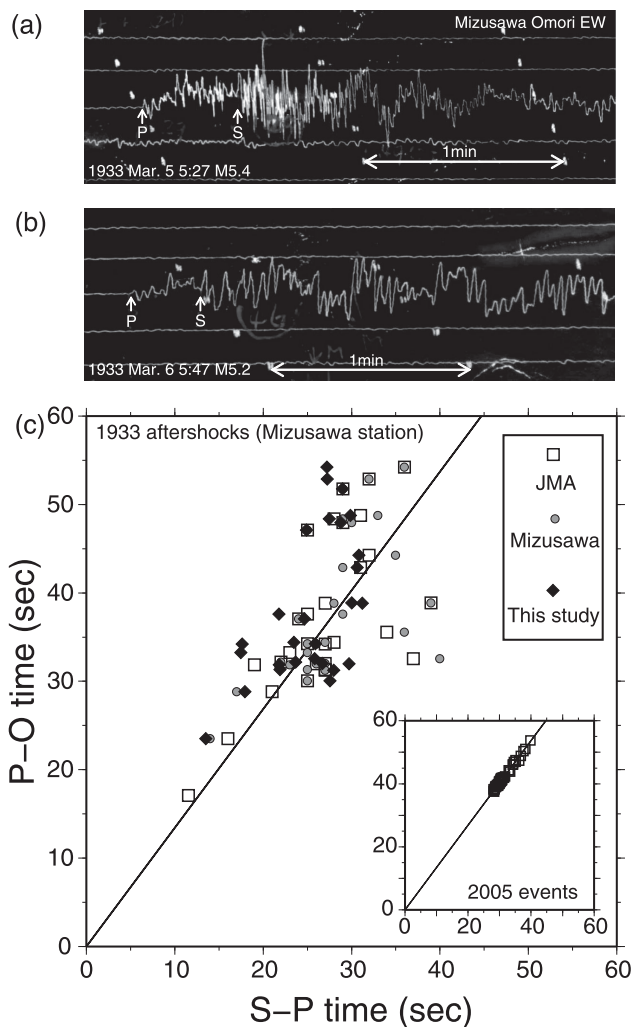


Figure 2. (a,b) Examples of two smoked-paper 1933 aftershock waveforms recorded at the Mizusawa station. The record was written on a 16-s-period E–W Omori type seismometer (45 kg mass weight). The JMA origin times are shown in the left bottom of each trace. (c) The S -wave/ P -wave arrival time difference versus P -wave arrival time – origin time at Mizusawa station for the 1933 aftershocks (1933 March 3 to May 24). The origin times are from the JMA catalogue. Squares, circles and diamonds are JMA phase data, the Mizusawa catalogue and our re-picked Mizusawa phase data, respectively. Right bottom inset is the same for the large figure but for the aftershocks of the 2005 M_w 7.0 outer-trench-slope earthquake (2007 May 5–31, Hino *et al.* 2009) recorded at several land stations. The black lines for both plots show a least-squares fit that corresponds to $V_p/V_s = 1.75$ for the 2005 aftershocks.

regional stations shows that the main-shock hypocentre is located inside the off-trench aftershock cloud (Fig. 3b). A 1-D velocity structure is also that used for the routine hypocentre determination of Tohoku University. The phase data are from JMA for all test relocations other than global ones that used those from the International Seismological Summary (ISS; Fig. 3e). The S – P time relocation method does not rely on the absolute timing of the P wave which may suffer from inaccurate timing of the stations. Here we used a grid search method to find the best-fit event locations to the observed S – P times. The results show that the main-shock hypocentres shifted slightly south and toward the trench. Aftershocks still ranged both to the east and west of the trench (Fig. 3c). The P -only relocation does not suffer from relatively inaccurate S -wave picking. However, this relocation result (Fig. 3d) is rather

scattered because of poor constraint on the distance from the network on land. Relocation using global teleseismic data with relatively good station coverage usually does not suffer as much from regional structure heterogeneity (Hino *et al.* 2009) because the seismic rays plunge downward where the subduction-related complexity is thought to be small. The relocation using global data was performed by the interactive iterative method of (Wyssession *et al.* 1991). The teleseismic main-shock location is closer to the trench compared with the JMA catalogue; aftershocks to the west of the trench are relocated relatively north (Fig. 3e). The detailed feature and implications are discussed in our companion paper (Okal *et al.* 2016). The relocation by the double difference method (Waldhauser & Ellsworth 2000) improves the relative location between events. The results show the main shock is located within the earthquake cloud in the off trench locations and the earthquake distribution is relatively tight.

Using these relocation methods we found that the main-shock epicentre is located inside the aftershock cloud off the trench except for the P -wave-only relocations that have relatively weak constraint on the distance from the seismic network (east-west direction). The aftershocks are located both east and west of the trench regardless the relocation method and which body-wave phase data were used (P , P and S , P – S).

4 SYSTEMATIC HYPOCENTRE MISLOCATION NEAR THE TRENCH AND CONSTRUCTION OF A 3-D VELOCITY STRUCTURE OFF SANRIKU

It is generally difficult to determine hypocentre depth accurately for shallow earthquakes occurring in the vicinity of a trench. Recent earthquake relocations by using OBS (ocean bottom seismometer) data near the Japan trench indicate large differences (~ 20 km) between well constrained OBS hypocentres and the hypocentres in the JMA or the Tohoku University's earthquake catalogue that are determined only from land seismic network data (Hino *et al.* 2000, 2009; Obana *et al.* 2012). These OBS locations provide accurate hypocentre locations in the near-trench region because the stations used for the relocations are located above the earthquake hypocentres and appropriate local velocity structures are used. Fig. 4(a) compares the epicentres from JMA (black dots) and OBS (collared dots) locations of events since 1992 (Hino *et al.* 2000, 2009; Obana *et al.* 2012) and Fig. 4(c) shows time residuals for each P phase at land stations by assuming the OBS hypocentre and origin time are correct (see the figure caption for the detail). The OBS locations tend to be west (landward) of apparent JMA's locations for events to the west of the trench (inner-trench-slope region) and tend to be east (seaward) of apparent JMA's locations for the events to the east of the trench (outer trench region). The positive observed minus calculated P -wave arrival times ($O - C$) for many events to the west of the trench suggest the actual averaged velocity along the path from the events to land station is slower than the 1-D velocity structure and the negative $O - C$ for events to the east of the trench suggest that the averaged velocity along the path from these events to the land stations is faster than the 1-D velocity structure. Therefore, we consider velocity heterogeneity in the offshore region is causing systematic shifts of the earthquake hypocentres determined by the land network using a commonly adopted 1-D velocity structure.

To incorporate this velocity heterogeneity, we construct a 3-D velocity structure and relocated earthquake by the structure. Previous

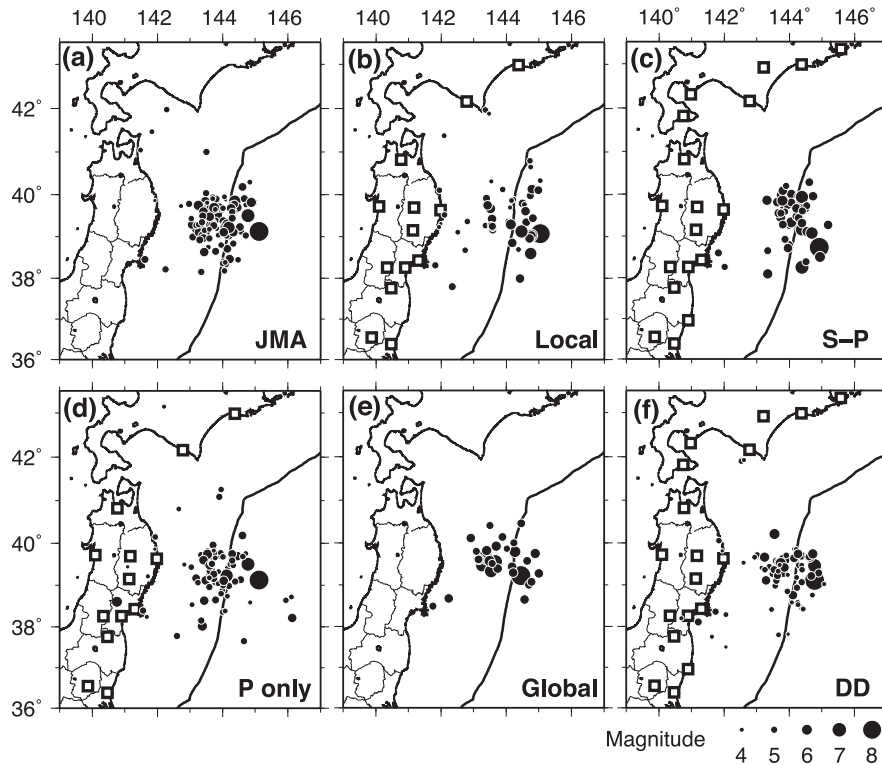


Figure 3. Epicentre distribution of the 1933 main shock and 3-month aftershocks. (a) JMA catalogue. (b) Relocation using phase data only from local stations and Tohoku-University's location routine that uses a 1-D velocity structure (Hasegawa *et al.* 1978). Epicentres with 0.5° or less error are selected here. (c) Relocation using a grid search of S - P times. (d) Relocation using local stations and Tohoku-University's routine 1-D velocity structure and only P waves. (e) Relocation P -wave phase data from global stations (Okal *et al.* 2016). (f) Relocation result using the double-difference method. In panels (b)–(d) and (f), the stations used for the relocation are shown by white squares. For all panels, the earthquake magnitudes are from the JMA catalogue.

seismic tomography and receiver function studies suggest, for the subducting plate, a faster subducting plate mantle (Tonegawa *et al.* 2006; Hino *et al.* 2009; Kawakatsu *et al.* 2009) and a slower offshore crust (Matsuzawa *et al.* 1987; Kawakatsu & Watada 2007; Tsuji *et al.* 2008; Yamamoto *et al.* 2008; Hino *et al.* 2009) compared to the average 1-D velocity structure beneath the Japanese island. Structure constraints from refraction and reflection experiments suggest a relatively shallow Moho and a faster mantle for the offshore forearc region (Ito *et al.* 2004; Ito *et al.* 2005). Using these constraints, we constructed a 3-D velocity structure as shown in Fig. 5. In this structure, we used the 3-D depth of the plate boundary (Nakajima & Hasegawa 2006; Kita *et al.* 2010) as a reference. The structure model consists of layers with seismic velocity that depends only the distance from the surface. Note that for the velocity within the subducting plate the distance from the subducting plate surface is used instead of the depth. For the crustal part of the subducting plate (0–15 km from the interplate surface), the velocity determined from the distance from the surface was increased with depth according to observed P -wave speed inferred from S-to-P converted waves (Shiina *et al.* 2013).

To test the relocation procedure using this 3-D velocity structure, we compared our locations of earthquakes with the locations based on OBS observations. Our relocation was performed by using land data only and the tomoFDD hypocentre relocation method (Zhang & Thurber 2003). Both earthquakes in the outer trench/outer rise region and inner trench region relocated closer to the OBS hypocentres (Fig. 6). The depths of the relocated earthquakes were greatly improved greatly by this procedure (Figs 6b and d). These results suggest that the use of a 3-D velocity structure greatly improves the absolute locations of these offshore earthquakes.

5 1933 HYPOCENTRE RELOCATIONS USING THE 3-D VELOCITY STRUCTURE

Fig. 7 and Supporting Information Table S1 show the 1933 main-shock and aftershock distribution before and after relocation using the foregoing procedure. Before relocation, the hypocentres are diffusely scattered, especially in depth and the main-shock hypocentre is located outside of the dense earthquake cluster. The relocation result shows that the earthquake distribution for both in the inner- and outer-trench-slope regions is largely shallow (depth ≤ 60 km below the sea level). Note that we adopted the hypocentre of main shock from global station data due to insufficient number of local phase data. The cross-section in the outer trench region shows that the aftershocks did not occur on a single plane. Red symbols show the events in the outer-trench area, which does not show simple fault plane. These earthquakes appear to be separated from the earthquakes in the offshore forearc region (black) by a relatively sparse seismicity region (Fig. 7c). To test this hypocentre distribution, we checked the waveforms for these events at Mizusawa station (Fig. 8a). The colour in Fig. 8 is coded according to the dominant frequency in the first 40 s window of the waveform. We determined the dominant frequency from the smoked-paper records by counting the number of peaks in the event time window. The distribution shows that high-frequency events are mostly located east of the trench and low frequency events tend to be located west of the trench region. Gamage *et al.* (2009) showed that the waveform characteristics are different for the hypocentres of recent events east and west of the trench. High frequency waveforms characterize earthquakes east of the Japan Trench and low-frequency

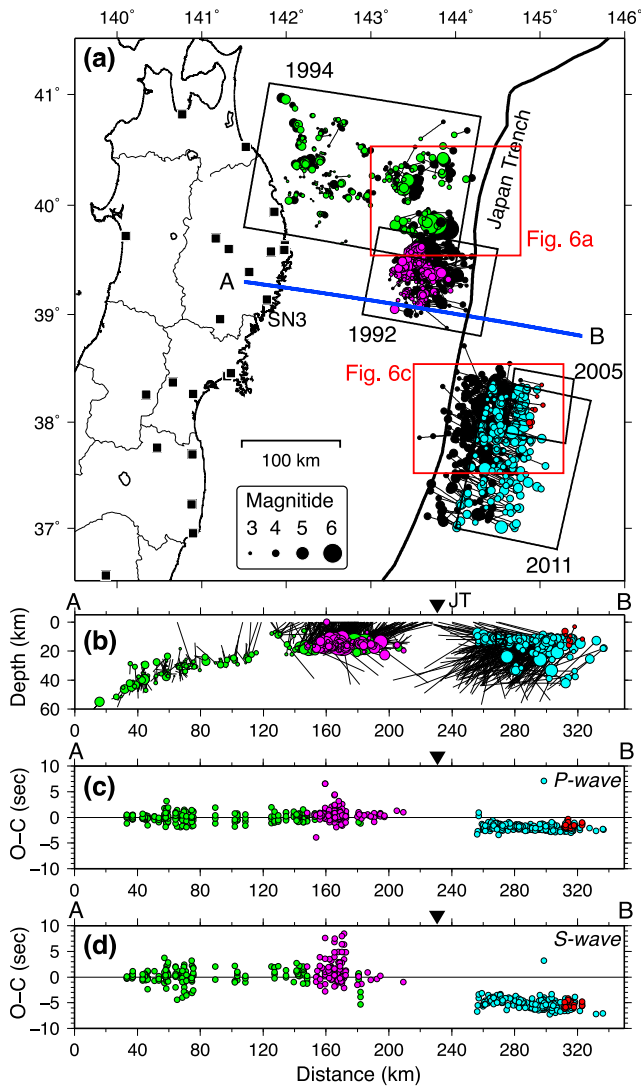


Figure 4. (a) Comparisons of the hypocentres from the JMA catalogue (black circles) and OBS relocations for the aftershocks of the 1992 M6.9 earthquake (Hino *et al.* 1996; pink), the 1994 M7.6 Sanriku-oki earthquake (Hino *et al.* 2000; green), the 2005 M7.0 earthquake (Hino *et al.* 2009; red) and the off-trench aftershocks of the 2011 M9.0 Tohoku earthquake and M7.6 outer-trench-slope earthquake (Obana *et al.* 2012). Rectangles show the selected regions where OBS stations were distributed in which the hypocentres are located with good accuracy. (b) Cross-section of hypocentres projected on trench-perpendicular line A–B shown in Fig. 4(a). The colours are the same as in panel (a). Thin lines join the OBS-relocated hypocentres (circle) with the hypocentres from the JMA catalogue. Inverted triangles show the position of the trench along this section. (c,d) Observed (*O*) minus Calculated (theoretical) (*C*) traveltimes as a function of the distance along the line A–B (a) for *P*-wave (c) and *S*-wave (d) readings. We plotted *O* – *C* for each phase data set obtained at the on-land stations (squares). For the calculation of (*O*), we used the JMA phase data and the OBS-relocated origin time. For the calculation of (*C*), we used 1-D routine velocity structure of Tohoku University (Hasegawa *et al.* 1978). Colours are the same as in panel (a).

waveforms characterize those earthquakes that locate west of the trench. We show the high-frequency and low-frequency earthquake examples for recent earthquakes in the supporting materials (Supporting Information Figs S1 and S2). The relationship applies very clearly to the dominant frequency of the 1933 aftershock and suggests that our locations relative to the trench position are accurate.

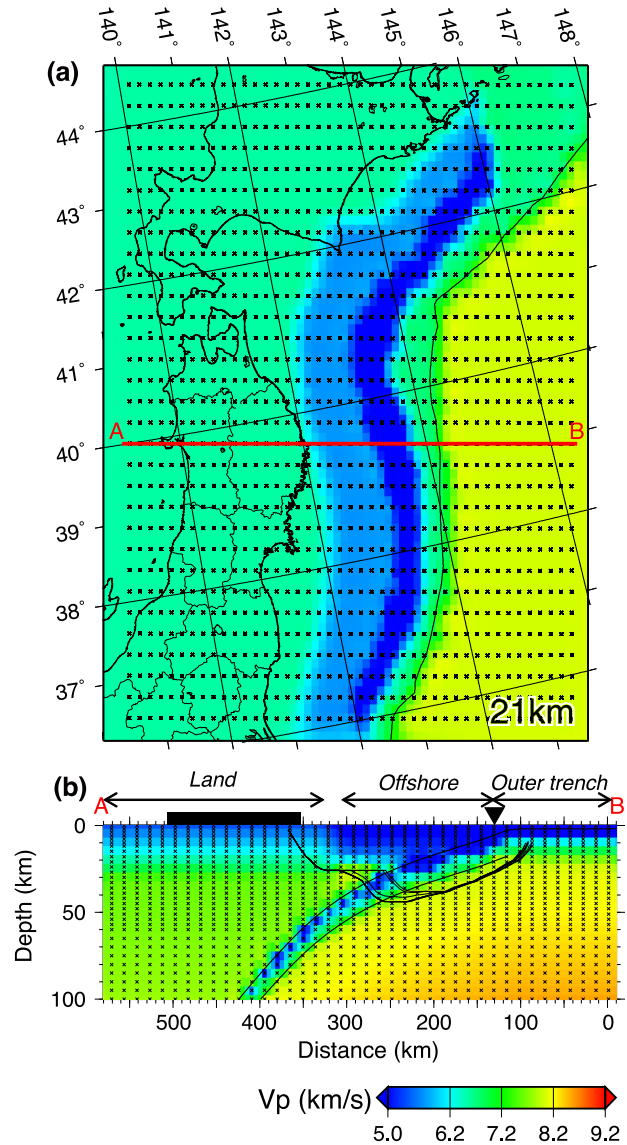


Figure 5. 3-D *P*-wave velocity structure used in this study based on marine and land velocity structure from Tohoku University investigation (Hasegawa *et al.* 1978; Hino *et al.* 2000, 2009). Small crosses show grid points. (a) The velocity along a depth section at 21 km. (b) Cross-section along the line A–B shown in (a). Land, offshore and outer trench slope show the areas where each 1-D velocity structure was used. Black curved line indicates the slab top surface. Thick black line and inverted triangle show land area and the Japan Trench, respectively.

Many aftershocks do indeed occur west of the trench. The activity of earthquakes show that the earthquakes to the west of the trench started to occur within 2 hours after the main shock (Figs 9a and b), suggesting the triggered seismicity started very early stage of the aftershock activities.

6 DISCUSSION

6.1 Triggering of the inner trench earthquakes

We found many earthquakes occurred beneath the inner-trench-slope region after the 1933 earthquake. To investigate the cause of these earthquakes in the megathrust zone, we estimated Coulomb stress change for interplate thrust earthquakes due to a giant

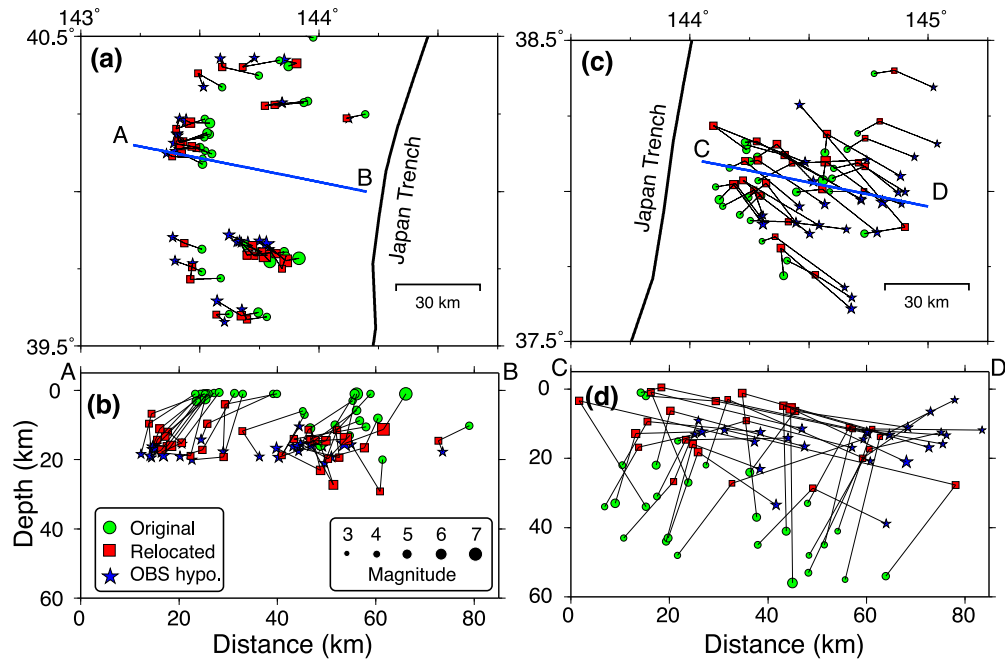


Figure 6. Comparisons of the relocated hypocentres using the 3-D velocity structure (red squares), OBS data (blue stars) and data from the original JMA catalogue (green circles). The hypocentres for the same event are connected by thin lines. Map view (a) and (b) cross-section along the line A–B of selected events under the inner trench slope. Earthquakes with M3.5 or larger that occurred after the 1994 M7.6 interplate earthquake are shown here. Map view (c) and (d) cross-section along the line C–D of selected off-trench earthquakes. Earthquakes that occurred after the 2005 M7.0 and 2011 M9.0 earthquakes are shown here. These two areas are also shown in Fig. 4(a).

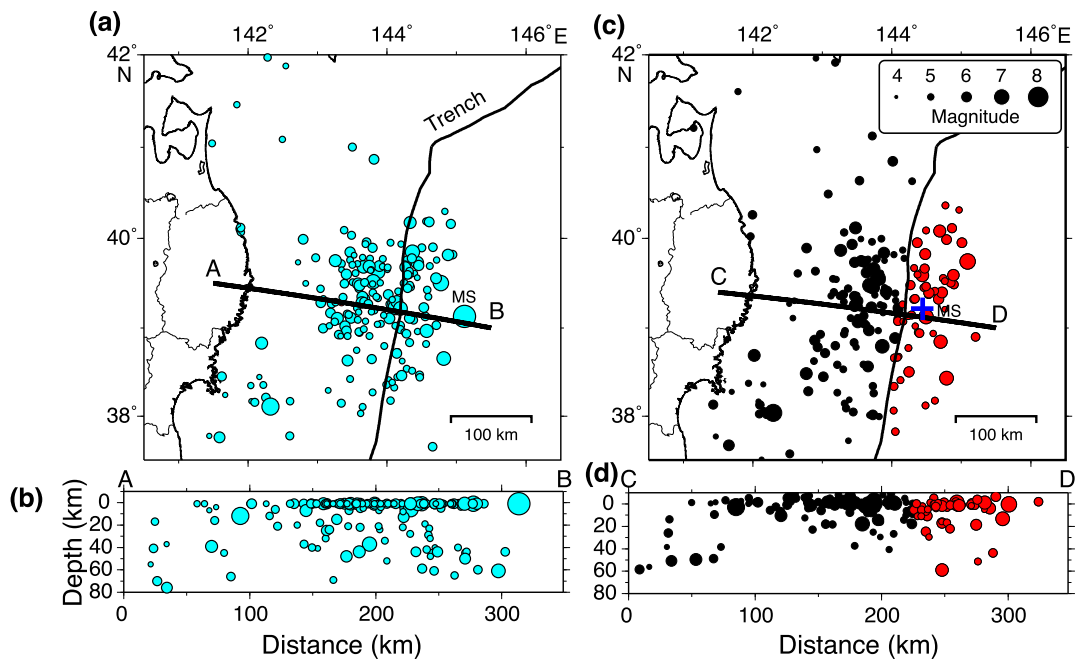


Figure 7. Hypocentre distribution of the 1933 main shock and its aftershocks. (a,b) JMA catalogue; (c,d) the results from our relocation by the 3-D velocity structure. Relocated epicentre of the main shock (cross) is from global stations. For panels (c) and (d), the red and black circles show hypocentres of outer trench and inner trench earthquakes, respectively.

off-trench normal faulting earthquake. Although the earthquake alignment in the cross-section is ambiguous due to small number of earthquakes and their scatter nearest the Japan trench, we take high angle (60° dip) rupture planes as working hypotheses. The bathymetry of the outer trench slope in this region shows both east-dipping and west-dipping high-angle fault scarps (Kobayashi *et al.* 1998) and Okal *et al.* (2016) estimated normal faulting earthquake

61° dip towards the trench. Low-angle normal fault plane (30° dip) that was suggested by Abe (1978) is mechanically very unfavourable and inconsistent with *P*-wave first motions for the 1933 earthquake. Considering wide distribution of trench-normal seismicity, single high dip-angle fault within shallow depth (depth ≤60 km) cannot cover all the epicentre in the outer-trench area. Therefore, we consider compound rupture of two normal faults facing with each

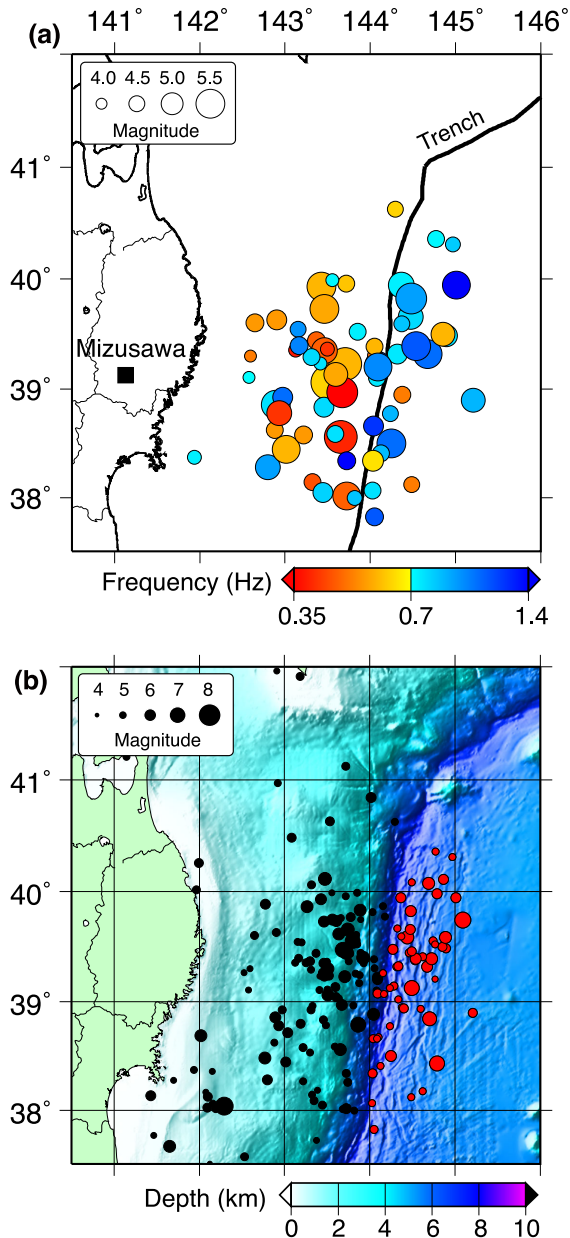


Figure 8. (a) Dominant frequency (colour) plotted at the location of the hypocentres. The black square shows the location of the seismic station (Mizusawa) where the dominant frequency was estimated from the waveforms recorded there. (b) Three months relocated aftershocks plotted on the bathymetry. Colours for the hypocentres are the same as in Fig. 7(c).

other in addition to single west-dipping normal. The compound rupture still satisfies the first motion observation of (Kanamori 1971) but with a steeper land-facing fault that is suggested by Okal *et al.* (2016). The compound rupture model have a 60 degree dip, a 58 km down-dip width and a 278 km fault plane length whose depth range extends from 10 to 60 km from sea level or 4 to 54 km below the seafloor, and conventional single fault model have the same dimensions (Fig. 10, rectangles). The average slip amounts are 4.5 and 9 m for the compound model and single model, respectively. The total moment is 4.3×10^{21} Nm for both models which is the same as Kanamori's model (Kanamori 1971) but smaller than more recent result [7×10^{21} Nm (Okal *et al.* 2016)]. Although there are difference in the moment, they does not affect to the spatial pattern

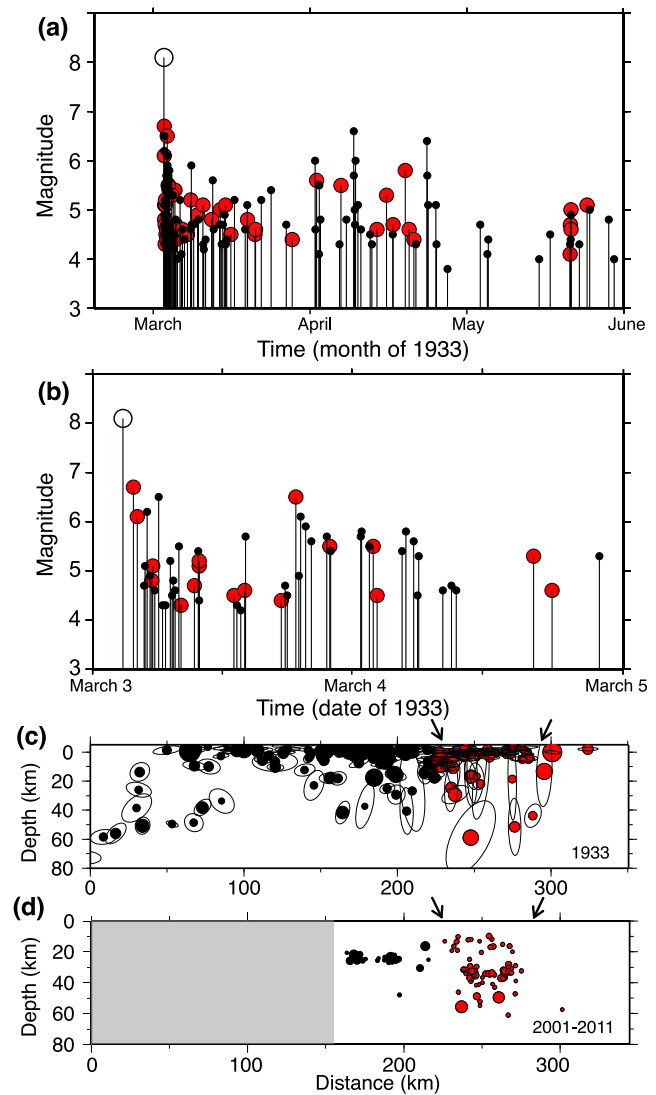


Figure 9. (a,b) Magnitude–time plot of relocated earthquakes. Colours are the same as in Figs 7(c,d) and 9(c). (c) Relocated earthquake locations with error ellipsoid in the same cross-section in Fig. 7(d). The error ellipsoid was estimated from 98 times relocations with bootstrap resampled residuals. Relocated earthquake locations for recent earthquakes from October 2001 to 2011 March 10. The location of the cross-section is the same as Fig. 9(c) and the band width is 20 km.

and polarity of the Coulomb stress change. This calculation was made using an elastic half-space following Okada (1992), assuming a shear modulus of 3.0×10^{10} N m⁻², a Poisson's ratio of 0.25, and an apparent coefficient of friction of 0.3. The Coulomb stress changes for thrust earthquakes on the plate boundary (Nakajima & Hasegawa 2006; Kita *et al.* 2010) show that events under the inner trench slope within 27 d after the 1933 earthquakes are mostly located in the area having positive stress changes from the compound model (Fig. 10a). There are large areas with Coulomb stress greater than the ~ 0.01 MPa, values which is the band of stress change that promotes seismicity in other tectonic settings (Stein *et al.* 1992; Harris *et al.* 1995; Toda *et al.* 1998). The single fault model also show positive Coulomb stress change near the trench where high aftershock seismicity occurred, but the contours with positive stress change greater than ~ 0.01 MPa do not contain all of the relocated aftershocks. Therefore, the spatial extent of aftershock is more consistent with compound rupture and suggests that the seismicity in

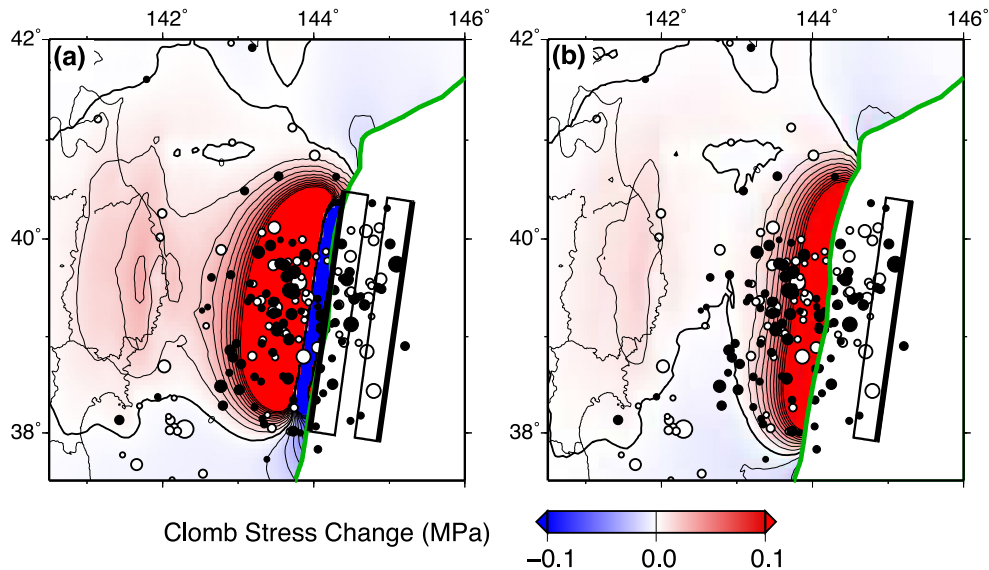


Figure 10. Changes in Coulomb failure stress on the plate boundary (colour-scale and contours) caused by two 60° normal faults shown by rectangles. The thick line is shallower edge of the faults. Panel (a) is for compound rupture of two normal faults dipping toward each other and panel (b) is for single west-dipping fault. The contour interval is 0.01 MPa; contours larger than 0.1 MPa are not drawn. For the calculation of the Coulomb failure stress change, the slip direction of the target earthquake is assumed to be parallel to the direction of relative plate motion. Black and white circles are relocated earthquakes that occurred from 1933 March 3 to 31 and 1933 April 1 to August 28, respectively.

the megathrust zone was probably triggered by the compound outer-trench-slope normal faulting. We now discuss in the next section these fault models in the context of the tsunami records.

6.2 Source faults and the tsunami paradox

To test the possibility of multiple faults in the shallow outer-trench-slope area, we calculated tsunami waveforms by solving the finite difference approximation of the linear long-wave equations (Satake 1995) for the compound-rupture model and single-fault model defined in the previous section.

Fig. 11 shows the bathymetry, fault models and tide-gauge observation points where we could obtain the near-field tide gauge records and its locations in 1933. The compound-rupture model and single-fault model corresponds to the rupture of faults A + B and fault B, respectively. The tide gauge records at Kushiro (KSR), Hachinohe (HCH) and Kesen-numa (KSN) (Sekiguchi & Nakano 1933) are digitized and corrected for curvature and inclination due to finite arm length. Then the tidal components are estimated by a moving window analysis and the components are removed from the tide gauge record to compare with the Tsunami modelling results. The observed tsunami waveform show small but clear upward first motions for HCH and KSN, located to the west of the source faults (Figs 12b and c). The first motion polarity at Kushiro, located to the north of the source faults is unclear due to relatively large noise to signal (Fig. 12a).

The tsunami calculation results for these stations show that the compound-rupture model can explain the upward first-motion polarity for HCH and KSN (Figs 12e and f). The overall features of waveforms at about 1 hour from the onset of Tsunami waves are also very similar except for their amplitudes for the compound-rupture model. On the other hand, the single-fault model cannot explain the tsunami first motions at HCH and KSN. The east dipping fault (Fault A) in the compound model closer to the Sanriku coast contributes an upward first motion of the tsunami waves that is a robust observation in the tide-gauge waveforms (Abe 1978). The tsunami

source model of (Hatori 1974) from back propagation of the tsunami suggest that western limit of the tsunami source is located not only in outer-trench-slope region but extends about 50 km west of the Japan trench. Thus, this also suggests that a single west-dipping fault (Fault b) cannot explain the tsunami waveforms well unless the fault is very close to the Japan trench or the fault dip is small.

Despite the similarity of the shape of the modelled Tsunami waveform with observation, the calculated amplitudes for the compound model are about 3–6 times larger than observations. The possibilities for the causing this discrepancy includes an assumption of too much slip (moment) for the earthquake, limitations of the frequency-responses of the tide gauges for short wavelength waves, or inadequate modelling of local bathymetry. Because this earthquake occurred early in the instrumental record, precise information on these limitations are not available. However we consider these cases do not affect the polarity of the initial tsunami wave that is a reliable feature for both observation and modelling by compound rupture model.

In Tohoku area, the occurrence of possible future off-trench earthquake triggered by M9 Tohoku-oki earthquake of 2011 is of concern. The automatic detection of compound rupture or doublet is still difficult (Beavan *et al.* 2010; Lay *et al.* 2010). If a subevent of a great earthquake closer to the land-area occurred simultaneously with the initial subevent further from the trench, it would cause earlier tsunami arrivals and in some cases larger tsunami waves on the coast than a single off-trench earthquake, an important scenario that we should keep in mind.

6.3 Depth limit of the rupture

Although the phase data for our relocations has an approximate 5 s standard error, the estimation of hypocentre uncertainty from a bootstrap method suggests that this shallow earthquake distribution is robust (Fig. 9c). 90 per cent of the aftershocks are located shallower than 18 km. The stress distribution in the oceanic lithosphere entering the deep sea trench is a superposition of bending

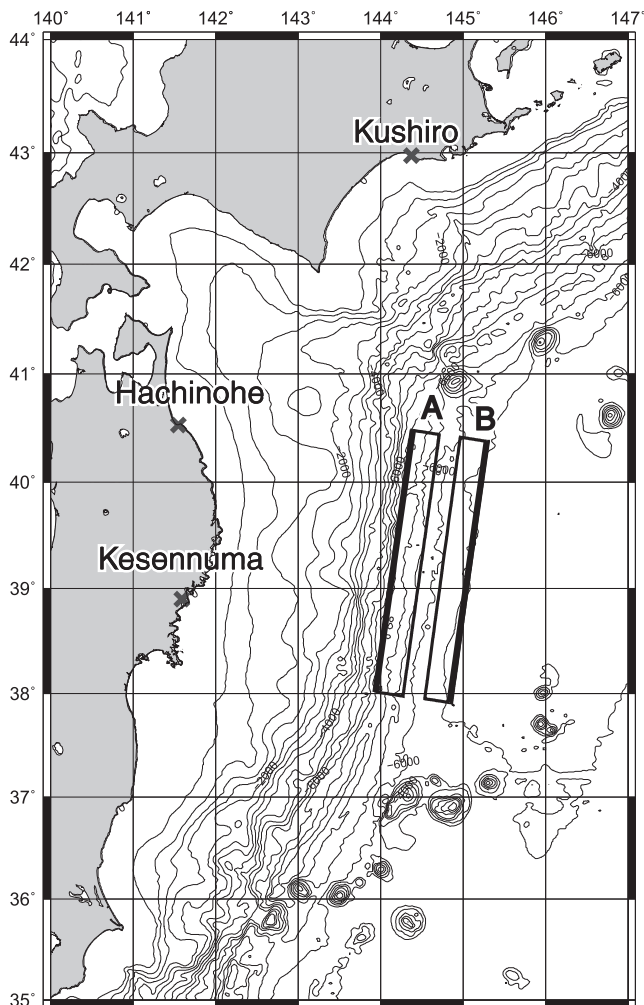


Figure 11. Distribution of tide gauge stations (cross), fault models (rectangles A and B) and bathymetry used for the theoretical tsunami calculations (contours).

forces, gravitational pull of cold sinking slab, and interplate locking along the megathrust boundary (Christensen & Ruff 1988). When considering the gravitational pull of cold sinking slab, a slab at the 50–200 km depth range in this subduction zone is not under deviatoric tension (Hasegawa *et al.* 1978; Yoshii 1979; Kawakatsu & Seno 1983; Kita *et al.* 2010). Bending produces a stress state with shallow extension and deeper compression. It seems unlikely that interplate locking acts as the cause of near-trench deviatoric tension because a locked interplate fault would tend to shelter the up-dip region from the slab-pull (Lay *et al.* 2010). In our study we found few reliable aftershocks (depth ≥ 50 km). Although rupturing without producing aftershocks may be possible, the aftershock distribution does not support full-plate offshore Pacific plate rupture. The aftershock distribution that we document suggests the whole lithosphere was not under deviatoric tension at the time of the 1933 earthquake.

6.4 Comparison with recent seismicity and bathymetry

We have compared the aftershock distribution of the 1933 earthquake with recent seismicity from October 2001 to 2011 March 10 that was relocated using the same procedure as we used for the aftershocks of the 1933 earthquake (Figs 13a and b). Here we selected the time period when the High-Sensitivity Seismograph Network

(Hi-net) phase data are available and the seismicity is not affected by the 2011 Tohoku-oki earthquake to obtain accurate and stable seismicity.

We subdivided and classified the off-trench region of the Japan Trench into numbered Group Sectors based on the morphologies and distributions of fault scarps in relation to the local orientation of the Japan Trench and orientations of magnetic anomalies that indicate the seafloor spreading fabric. Such structural fabric can be reactivated in the zone of deformation near trenches (Masson 1991; Kobayashi *et al.* 1998). To do this, we relied upon the paper by Masao Nakanishi (2011) who mapped the off-trench normal fault scarps seaward of the Japan and Kuril Trenches, their spacings, the directions that these scarps dip, and their fault throws along selected profiles. Nakanishi's work was based on swath mapping data collected from various sources. Kobayashi *et al.* (1998) also noted the abrupt change in fault-scarp orientations, spacing, and average scarp throws between Group Sectors 3 and 4 with the Group Sector 4 scarps being attributed to reactivation of Pacific-Plate brittle weakness parallel to the seafloor spreading fabric. We point out that the Group 3 Sector is where most of the off-trench 1933 aftershocks occurred and where narrow near-trench bands of present-day earthquakes have also occurred near the trench. The \sim trench-parallel horst and graben structure in this Sector 3 indicates that both ocean-ward and trench-ward dipping faulting occur in this sector and that maximum fault throws approach 500 m near the Japan Trench.

Recent seismicity is largely shallow (depth ≤ 60 km below the sea level) and also consistent these four sector groupings of earthquakes along the trench based on fault scarp morphology (Fig. 13a). The 6-month aftershocks of the 1933 earthquake (red circles in Fig. 13b) are mainly distributed in Group 3 where the recent earthquakes are relatively concentrated near the trench (Fig. 13a, black circles in Fig. 13b). In this region there are several trench-parallel alignments of seismicity. This linear trend at shallow depths was also reported using OBS locations in 1981 by Kasahara *et al.* (1982). As noted above the bathymetry in this region shows largely trench parallel horst-and-graben fault scarps (Fig. 8b) a structure that is in consistent with our 1933 earthquake's fault models. Kobayashi *et al.* (1998) suggests that the crust is weakest along the inherited spreading fabric, second weakest probably along the non-transform offset direction and strongest in directions very oblique to these orientations. The fault scarps and trench-parallel bands of earthquakes crosscut the spreading fabric at angles as high as 58° in the latitude range for the 1933 aftershocks indicating that the 1933 rupture and subsequent seismogenesis has occurred on faults that were newly created in the off-trench region with total normal fault throws approaching 500 m near the trench axis (Nakanishi 2011). We have investigated the fine structure of recent earthquakes in the Group 3 Sector and show a cross section of the hypocentres of these events that includes the hypocentre of the 1933 main shock (Fig. 9d). This cross section resembles the cross section of our 1933 main shock (Fig. 9c), but with many more events. We recognize multiple fault-like alignments evident in both the epicentres of off-trench earthquakes in trench parallel bands (Fig. 13a) and in cross sections of hypocentres that were relocated using the same procedure that we used in relocating the 1933 aftershocks. In particular we point out multiple alignments of modern hypocentres into steeply dipping fault-like structures, including one such alignment is closest to the trench that dips seaward. Obana *et al.* (2016 and personal communications in May 2016) also reported two such trench-parallel bands of seismicity and a seaward-dipping structure in preliminary locations of off-trench earthquakes detected by a two-month OBS

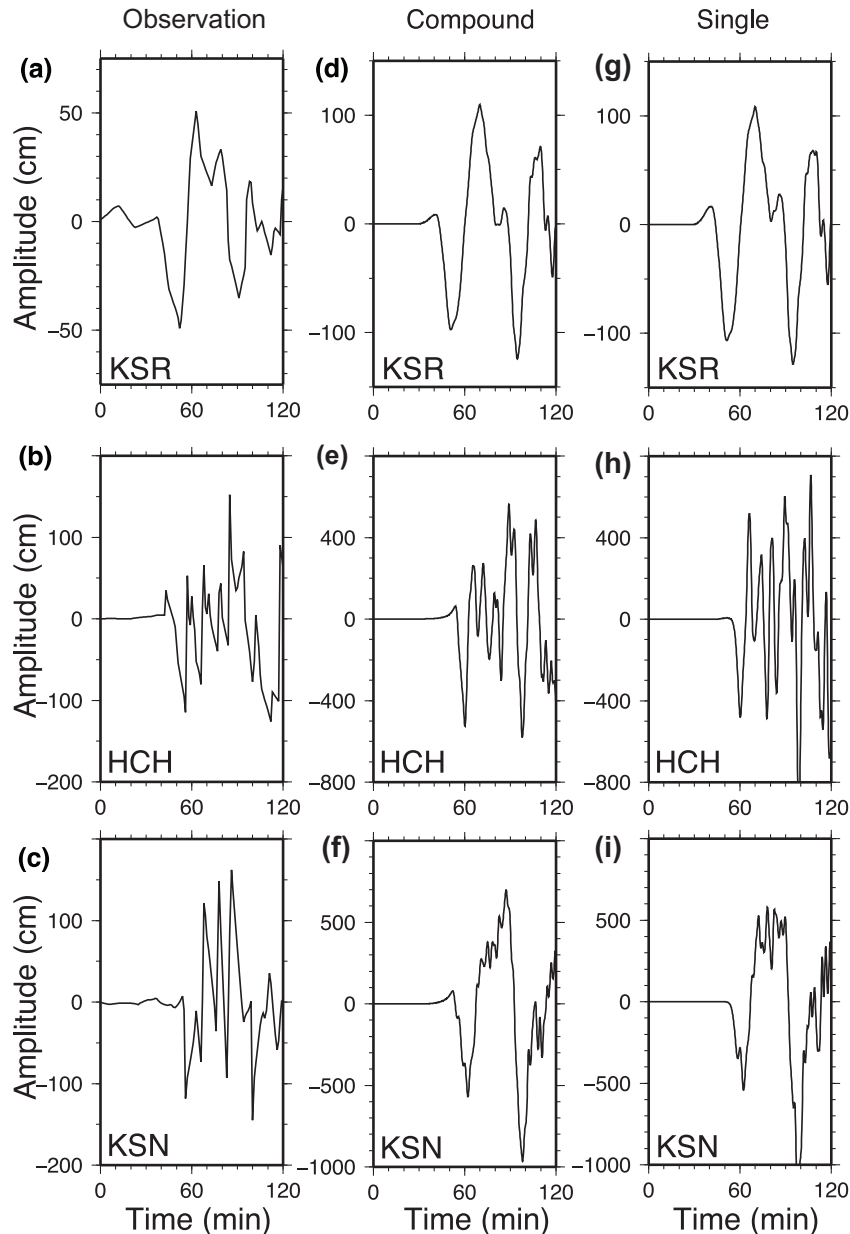


Figure 12. Observed and calculated tsunami waveforms for Kushiro (KSR), Hachinohe (HCH) and Kesen-numa (KSN) tide gauge stations. (a–c) Observed waveforms after the correction for curvature and inclination due to the finite arm length and subtracting the tidal components. (d–f) Theoretical waveform from a compound rupture model. (g–i) Theoretical waveform for a single fault model.

deployment in late summer of 2015. He and his colleagues interpreted these fault-like alignments, as we do, are possibly continuing aftershocks of the great 1933 Sanriku-oki earthquake more than 80 years after the earthquake and disastrous tsunami (Obana *et al.* 2016). The foregoing interpretation of a two-fault compound source with ruptures dipping toward each other for the 1933 main shock and aftershocks and present-day off-trench earthquakes is obviously of a simplification of a more complex distributed extensional regime in the outer rise and inner trench slope of the 1933 source region. Until we have long-term deep-water OBS deployments in the off-trench region of the Group 3 Sector and detailed seismic reflection and coring in that area to test this model, it should be considered provisional.

That such aftershocks could still be occurring is remarkable and is consistent with long-duration aftershocks of large intraplate earth-

quakes in the distributed deformation in continental interiors where average loading rates are very low (Stein & Liu 2009). Their paper gives insights into long-duration aftershocks using rate-and-state friction theory by equating low stressing rates with low average slip rates in such regions. Kirby (2016, unpublished data) has estimated average slip rates of about 0.5 mm yr^{-1} in the Sanriku source region based on the evolution of scarp heights during the time interval from the Pacific Plate moving over the outer rise to the trench at the latitude of the 1933 main shock at 39.2° . The Stein and Liu model indicated aftershock durations of centuries for great earthquakes for the low average slip rates in our setting. A slow rate of decay of seismicity rate of 1933 aftershocks is also consistent with nearly constant seismicity rates evident after just a couple of months in 1933 (Figs 13a and b). In our view, the occurrence of fault-like alignments of modern off-trench earthquake hypocentres re-enforces our

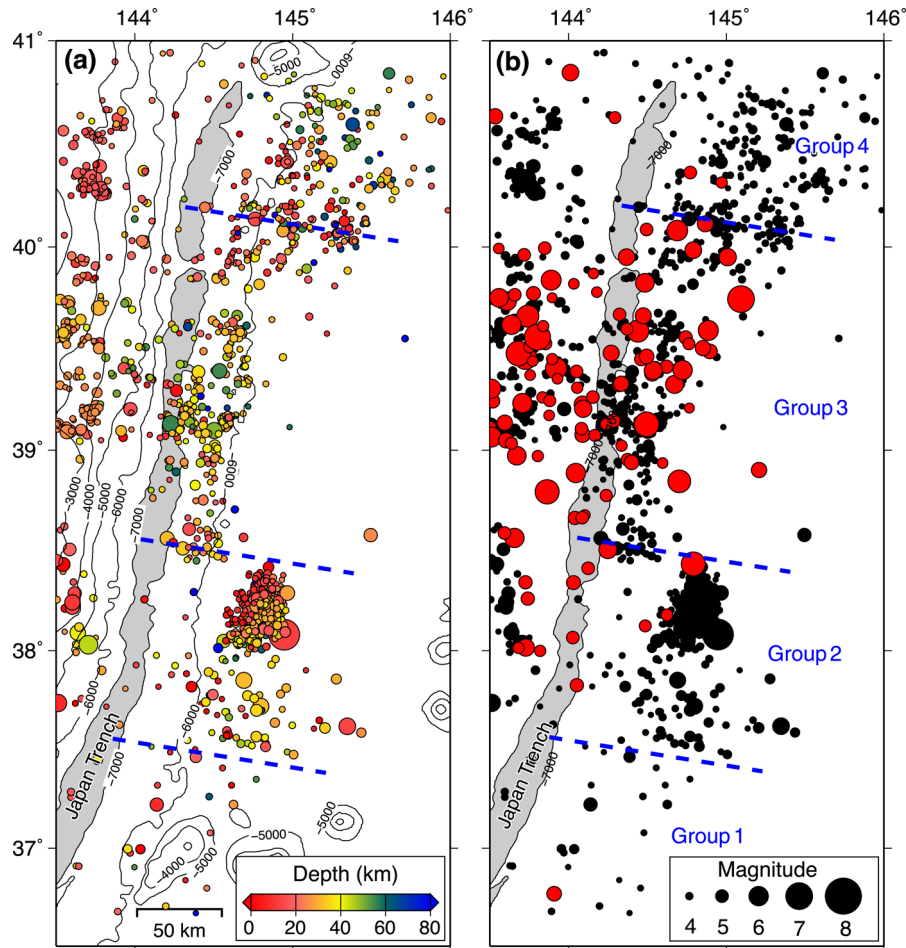


Figure 13. Comparison of the relocated 1933 aftershock epicentres and recent seismicity. (a) Epicentre distribution of recent earthquakes from October 2001 to 2011 March 10 (circle). The circles are colour coded according to hypocentral depth. (b) The comparison of the epicentre distribution of recent earthquakes (black circles) and the 6-month aftershocks of the 1933 earthquake (red circles). Grey area shows the area with seafloor depths ≥ 7000 m defining the position of the Japan Trench. Contours in panel (a) represent seafloor depths in 1000 m intervals. Note that the recent Group 2 off-trench events are located in the same band of seismicity as the 1933 aftershocks. Note the sharp boundaries between Group 3 and Groups 2 and 4.

interpretation of very sparse 1933 aftershock hypocentres that both seaward-dipping and oceanward-dipping faulting to depths exceeding 50 km occurred during the 1933 main-shock rupture. The relocated epicentre and focal mechanism based on first motions and waveform modelling (Okal *et al.* 2016) indicate that the initial main-shock rupture was probably trench-ward dipping at about 60° and located in the band of off-trench earthquakes most seaward of the trench, but that its moment tensor was also consistent with the total moment release from a compound rupture. As we discussed earlier in this paper, the upward first motion of the tide-gage records of the tsunami waves also point to an ocean-ward-dipping rupture nearest the trench and Japan coastline as a part of this compound earthquake and tsunami source.

7 CONCLUSIONS

Land-station based hypocentre determinations by using 3D velocity structure was applied in this paper to the off-Sanriku near-trench earthquakes where systematic hypocentre mislocations are recognized in the previous studies. The improvement of hypocentre locations were confirmed by an examination of recent earthquakes that are more accurately located based on OBS data above the study area. Aftershocks that occurred just after the 1933 Sanriku-oki main

shock are located in a roughly 280-km-long zone in the off-trench region that is separated from the aftershock seismicity under the marine forearc trench slope. The off-trench earthquakes are shallow (depth ≤ 50 km) and at a maximum depth below the seafloor of about 43 km. There are west dipping and east dipping earthquake alignments in the trench-normal cross-section. Although the aftershock depth distribution is not closely constrained, the shallow aftershock distribution suggests a shallow rupture depth range and possibly a compound rupture for the 1933 main shock. We found the compound rupture model explains better the polarity of tsunami waves at the Sanriku coast than a single west-dipping normal fault and better fits the Coulomb stress change in relation to aftershock locations the west of the trench. The occurrence of aftershocks both east and west of the trench was confirmed by an investigation of waveform frequency differences between these two classes of shallow earthquakes which is also seen in more recent earthquakes with better location accuracies. The relocated earthquakes under the offshore forearc are shallow (depth ≤ 30 km) and occur where recent activity of interplate thrust earthquakes is high. This suggests the deformation of the 1933 outer-rise earthquake triggered interplate earthquakes by a stress transfer process. Recent (2001–2012) seismicity in the 1933 off-trench source area relocated by the same method shows that the present seismicity in the off-trench region of

northern Honshu can be divided into several groups of earthquakes along the trench; one group roughly corresponds to the locations of the off-trench aftershocks of the 1933 earthquake. Comparison of the 1933 rupture dimensions based on our relocations with the morphologies of fault scarps in the outer trench slope suggest that the rupture was largely limited to the region where fault scarps are trench parallel and cross cut seafloor spreading fabric. These suggest bending and along-strike structural segmentation largely controls the horizontal and vertical extent of the fault. The triggering of interplate seismicity suggests that the great outer-rise/outer-trench-slope earthquake environment is closely linked to the earthquake cycle of interplate earthquake. The depth extent for this largest outer rise/outer-trench-slope earthquake also provides a constraint on the stress state of the subducting plate and the water transported to deep Earth into the subducting slab.

ACKNOWLEDGEMENTS

We thank the International Latitude Observatory of Mizusawa, Yoshiaki Tamura and Toshio Kono for smoked-paper seismogram images of the 1933 aftershocks, and the Japan Meteorological Agency for earthquake phase data. We also thank E. Okal for the discussion on the hypocentre relocation and providing hypocentre relocation results by global station data, K. Obana for providing us the hypocentres of off-trench earthquakes based on OBS observations, S. Kita for providing programs for constructing offshore velocity structure and earthquake relocations, M. Okada for the locations of tide gauge stations in 1933, Y. Tanioka for the assistance in digitizing the tsunami waves, and W. Ellsworth, T. Matsuzawa, A. Hasegawa and H. Kanamori for discussion. Some of the figures were drawn using Generic Mapping Tools software (Wessel & Smith 1995).

REFERENCES

- Abe, K., 1978. A dislocation model of the 1933 Sanriku earthquake consistent with the tsunami waves, *J. Phys. Earth*, **26**, 381–396.
- Aida, I., 1977. Simulations of large tsunamis occurring in the past off the coast of the Sanriku district, *Bull. Earthq. Res. Inst. Univ. Tokyo*, **52**, 71–101.
- Asano, Y. *et al.*, 2011. Spatial distribution and focal mechanisms of aftershocks of the 2011 off the Pacific coast of Tohoku Earthquake, *Earth Planets Space*, **63**, 669–673.
- Beavan, J., Wang, X., Holden, C., Wilson, K., Power, W., Prasetya, G., Bevis, M. & Kautoke, R., 2010. Near-simultaneous great earthquakes at Tongan megathrust and outer rise in September 2009, *Nature*, **466**, 959–963.
- Christensen, D.H. & Ruff, L.J., 1988. Seismic coupling and outer rise earthquakes, *J. geophys. Res.*, **93**, 13 421–13 444.
- Fujiwara, T., Kodaira, S., No, T., Kaiho, Y., Takahashi, N. & Kaneda, Y., 2011. The 2011 Tohoku-Oki earthquake: displacement reaching the trench axis, *Science*, **334**, 1240.
- Garage, S.S.N., Umino, N., Hasegawa, A. & Kirby, S.H., 2009. Offshore double-planed shallow seismic zone in the NE Japan forearc region revealed by sP depth phases recorded by regional networks, *Geophys. J. Int.*, **178**, 195–214.
- Harris, R.A., Simpson, R.W. & Reasenber, P.A., 1995. Influence of static stress changes on earthquake locations in southern California, *Nature*, **375**, 221–224.
- Hasegawa, A. & Nakajima, J., 2004. Geophysical constraints on slab subduction and arc magmatism, in *The State of the Planet: Frontiers and Challenges in Geophysics*, pp. 81–93, eds Sparks, R.S.J. & Hawkesworth, C.J., AGU.
- Hasegawa, A., Umino, N. & Takagi, A., 1978. Double-planed structure of the deep seismic zone in the northeastern Japan arc, *Tectonophysics*, **47**, 43–58.
- Hatori, T., 1974. Tsunami sources on the Pacific side in northeast Japan, *Zisin(2)*, **27**, 321–337.
- Hino, R., Kanazawa, T. & Hasegawa, A., 1996. Interplate seismic activity near the northern Japan Trench deduced from ocean bottom and land-based seismic observations, *Phys. Earth planet. Inter.*, **93**, 37–52.
- Hino, R., Ito, S., Shiobara, H., Shimamura, H., Sato, T., Kanazawa, T., Kasahara, J. & Hasegawa, A., 2000. Aftershock distribution of the 1994 Sanriku-oki earthquake (M_w 7.7) revealed by ocean bottom seismographic observation, *J. geophys. Res.*, **105**, 21 697–21 710.
- Hino, R. *et al.*, 2009. Insight into complex rupturing of the immature bending normal fault in the outer slope of the Japan Trench from aftershocks of the 2005 Sanriku earthquake ($M_w = 7.0$) located by ocean bottom seismometry, *Geochem. Geophys. Geosyst.*, **10**, Q07O18, doi:10.1029/2009GC002415.
- Inuma, T., Ohzono, M., Ohta, Y. & Miura, S., 2011. Coseismic slip distribution of the 2011 off the Pacific coast of Tohoku Earthquake (M 9.0) estimated based on GPS data—Was the asperity in Miyagi-oki ruptured?, *Earth Planets Space*, **63**, 643–648.
- Inuma, T. *et al.*, 2012. Coseismic slip distribution of the 2011 off the Pacific Coast of Tohoku Earthquake (M 9.0) refined by means of seafloor geodetic data, *J. geophys. Res.*, **117**, doi:10.1029/2012JB009186.
- Ito, A., Fujie, G., Tsuru, T., Kodaira, S., Nakanishi, A. & Kaneda, Y., 2004. Fault plane geometry in the source region of the 1994 Sanriku-oki earthquake, *Earth planet. Sci. Lett.*, **223**, 163–175.
- Ito, A., Fujie, G., Miura, S., Kodaira, S., Kaneda, Y. & Hino, R., 2005. Bending of the subducting oceanic plate and its implication for rupture propagation of large interplate earthquakes off Miyagi, Japan, in the Japan Trench subduction zone, *Geophys. Res. Lett.*, **32**, L05310, doi:10.1029/2004GL022307.
- Ivancic, M., Grevemeyer, I., Berhorst, A., Flueh, E.R. & McIntosh, K., 2008. Impact of bending related faulting on the seismic properties of the incoming oceanic plate offshore of Nicaragua, *J. geophys. Res.*, **113**, B05410, doi:10.1029/2007JB005291.
- Iwamori, H., 2000. Deep subduction of H₂O and deflection of volcanic chain towards backarc near triple junction due to lower temperature, *Earth planet. Sci. Lett.*, **181**, 41–46.
- Kanamori, H., 1971. Seismological evidence for a lithospheric normal faulting — the Sanriku earthquake of 1933, *Phys. Earth planet. Inter.*, **4**, 289–300.
- Kanamori, H. & Press, F., 1970. How thick is the lithosphere?, *Nature*, **226**, 330–331.
- Kasahara, J., Nagumo, S., Koresawa, S., Nishi, Y. & Sugimoto, H., 1982. A linear trend of hypocenter distribution in the outer slope region of the Japan Trench revealed by OBS array: preliminary report, *Bull. Earthq. Res. Inst. Univ. Tokyo*, **57**, 83–104.
- Kawakatsu, H. & Seno, T., 1983. Triple seismic zone and the regional variation of seismicity along the Northern Honshu Arc, *J. geophys. Res.: Solid Earth*, **88**, 4215–4230.
- Kawakatsu, H. & Watada, S., 2007. Seismic evidence for deep-water transportation in the mantle, *Science*, **316**, 1468–1471.
- Kawakatsu, H., Kumar, P., Takei, Y., Shinohara, M., Kanazawa, T., Araki, E. & Suyehiro, K., 2009. Seismic evidence for sharp lithosphere-asthenosphere boundaries of oceanic plates, *Science*, **324**, 499–502.
- Kirby, S., Engdahl, R.E. & Denlinger, R., 1996. Intermediate-depth intraslab earthquakes and arc volcanism as physical expressions of crustal and uppermost mantle metamorphism in subducting slabs, in *Subduction Top to Bottom*, pp. 195–214, eds Bebout, G.E., Scholl, D.W., Kirby, S.H. & Platt, J.P., AGU.
- Kita, S., Okada, T., Nakajima, J., Matsuzawa, T. & Hasegawa, A., 2006. Existence of a seismic belt in the upper plane of the double seismic zone extending in the along-arc direction at depths of 70–100 km beneath NE Japan, *Geophys. Res. Lett.*, **33**, doi:10.1029/2006GL028239.
- Kita, S., Okada, T., Hasegawa, A., Nakajima, J. & Matsuzawa, T., 2010. Existence of interplane earthquakes and neutral stress boundary between

- the upper and lower planes of the double seismic zone beneath Tohoku and Hokkaido, northeastern Japan, *Tectonophysics*, **496**, 68–82.
- Kobayashi, K., Nakanishi, M., Tamaki, K. & Ogawa, Y., 1998. Outer slope faulting associated with the western Kuril and Japan trenches, *Geophys. J. Int.*, **134**, 356–372.
- Koyama, J., Horiuchi, S. & Hirasawa, T., 1973. Earthquake generating stress in north-east Japan arc inferred from superposition of the initial motions of *P*-waves, *Zisin(2)*, **26**, 241–253.
- Kunitomi, S., 1933. On the Sanriku-oki strong motion and Tsunami, *Kenshin-jihou*, **7**, 1–43.
- Lay, T., Ammon, C.J., Kanamori, H., Rivera, L., Koper, K.D. & Hutko, A.R., 2010. The 2009 Samoa-Tonga great earthquake triggered doublet, *Nature*, **466**, 964–968.
- Lay, T., Ammon, C.J., Kanamori, H., Kim, M.J. & Xue, L., 2011. Outer trench-slope faulting and the 2011 M_w 9.0 off the Pacific coast of Tohoku earthquake, *Earth Planets Space*, **63**, 713–718.
- Lefeldt, M., Grevemeyer, I., Göbner, J. & Bialas, J., 2009. Intraplate seismicity and related mantle hydration at the Nicaraguan trench outer rise, *Geophys. J. Int.*, **178**, 742–752.
- Masson, D.G., 1991. Fault patterns at outer trench walls, *Mar. Geophys. Res.*, **13**, 209–225.
- Matsuzawa, T., Umino, N., Hasegawa, A. & Takagi, A., 1987. Estimation of thickness of a low-velocity layer at the surface of the descending oceanic plate beneath the northeastern Japan arc by using synthesized *PS*-wave, *Tohoku Geophys. J.*, **31**, 19–28.
- Nakajima, J. & Hasegawa, A., 2006. Anomalous low-velocity zone and linear alignment of seismicity along it in the subducted Pacific slab beneath Kanto, Japan: reactivation of subducted fracture zone?, *Geophys. Res. Lett.*, **33**, doi:10.1029/2006GL026773.
- Nakajima, J., Tsuji, Y. & Hasegawa, A., 2009. Seismic evidence for thermally-controlled dehydration reaction in subducting oceanic crust, *Geophys. Res. Lett.*, **36**, L03303, doi:10.1029/2008GL036865.
- Nakanishi, M., 2011. Bending-related topographic structures of the subducting plate in the Northwestern Pacific Ocean, in *Accretionary Prisms and Convergent Margin Tectonics in the Northwest Pacific Basin*, pp. 1–38, eds Ogawa, Y., Anma, R. & Dilek, Y., Springer.
- Obana, K. *et al.*, 2012. Normal-faulting earthquakes beneath the outer slope of the Japan Trench after the 2011 Tohoku earthquake: implications for the stress regime in the incoming Pacific plate, *Geophys. Res. Lett.*, **39**, L00G24, doi:10.1029/2011GL050399.
- Obana, K., Nakamura, Y., Kaiho, Y., Yamamoto, Y., Kodaira, S. & Fujie, G., 2016. Seismicity observations in the source region of the 1896 Meiji-Sanriku and 1933 Showa-Sanriku Earthquakes, in *JpGU 2016 Meeting*, SSS02-14.
- Okada, Y., 1992. Internal deformation due to shear and tensile faults in a half-space, *Bull. seism. Soc. Am.*, **82**, 1018–1040.
- Okal, E.A., Kirby, S.H. & Kalligeris, N., 2016. The Showa Sanriku earthquake of 02 March 1933: a global seismological reassessment, *Geophys. J. Int.*, in press, doi:10.1093/gji/ggw206.
- Peacock, S.M., 2001. Are the lower planes of double seismic zones caused by serpentine dehydration in subducting oceanic mantle?, *Geology*, **29**, 299–302.
- Ranero, C.R., Phipps Morgan, J., McIntosh, K. & Reichert, C., 2003. Bending-related faulting and mantle serpentinization at the Middle America trench, *Nature*, **425**, 367–373.
- Satake, K., 1995. Linear and nonlinear computations of the 1992 Nicaragua earthquake tsunami, *Pure appl. Geophys.*, **144**, 455–470.
- Sekiguchi, R. & Nakano, M., 1933. Report on Sanriku Tsunami based on tide gauge, *Kenshin-jihou*, **7**, 71–79.
- Seno, T. & Gonzalez, D.G., 1987. Faulting caused by earthquakes beneath the outer slope of the Japan Trench, *J. Phys. Earth*, **35**, 381–407.
- Shiina, T., Nakajima, J. & Matsuzawa, T., 2013. Seismic evidence for high pore pressures in the oceanic crust: implications for fluid-related embrittlement, *Geophys. Res. Lett.*, **40**, 2006–2010.
- Stein, R.S., King, G.C.P. & Lin, J., 1992. Change in failure stress on the Southern San Andreas fault system caused by the 1992 magnitude = 7.4 Landers earthquake, *Science*, **258**, 1328–1332.
- Stein, S. & Liu, M., 2009. Long aftershock sequences within continents and implications for earthquake hazard assessment, *Nature*, **462**, 87–89.
- Tanioka, Y. & Satake, K., 1996. Fault parameters of the 1896 Sanriku Tsunami Earthquake estimated from tsunami numerical modeling, *Geophys. Res. Lett.*, **23**, 1549–1552.
- The Central Meteorological Observatory, 1933. Damage investigation of the Sanriku Tsunami, *Kenshin-jihou*, **7**, 105–159.
- The International Latitude Observatory of Mizusawa, 1984. *Seismological Observations at Mizusawa for the Period Between 1902–1967*, Mizusawa-insatsu.
- Toda, S., Stein, R.S., Reasenber, P.A., Dieterich, J.H. & Yoshida, A., 1998. Stress transferred by the 1995 M_w = 6.9 Kobe, Japan, shock: effect on aftershocks and future earthquake probabilities, *J. geophys. Res.*, **103**, 24 543–24 565.
- Todd, E.K. & Lay, T., 2013. The 2011 Northern Kermadec earthquake doublet and subduction zone faulting interactions, *J. geophys. Res.*, **118**, 249–261.
- Tongewa, T., Hirahara, K., Shibutani, T. & Fujii, N., 2006. Lower slab boundary in the Japan subduction zone, *Earth planet. Sci. Lett.*, **247**, 101–107.
- Tsuji, Y., Nakajima, J. & Hasegawa, A., 2008. Tomographic evidence for hydrated oceanic crust of the Pacific slab beneath northeastern Japan: implications for water transportation in subduction zones, *Geophys. Res. Lett.*, **35**, L14308, doi:10.1029/2008GL034461.
- Umino, N. *et al.*, 2006. Revisiting the three $M \sim 7$ Miyagi-oki earthquakes in the 1930s: possible seismogenic slip on asperities that were re-ruptured during the 1978 $M7.4$ Miyagi-oki earthquake, *Earth Planets Space*, **58**, 1587–1592.
- Waldhauser, F. & Ellsworth, W.L., 2000. A double-difference earthquake location algorithm: method and application to the Northern Hayward Fault, California, *Bull. seism. Soc. Am.*, **90**, 1353–1368.
- Wartman, J.M., Kita, S., Kirby, S.H. & Choy, G.L., 2009. A global outer-rise/outer-trench-slope (OR/OTS) earthquake study, in *American Geophysical Union, Fall Meeting 2009 abstract*, #S53A-1472.
- Wessel, P. & Smith, W.H.F., 1995. New version of generic mapping tools released, *EOS, Trans. Am. geophys. Un.*, **79**, 329.
- Wyssession, M., Okal, E. & Miller, K., 1991. Intraplate seismicity of the Pacific Basin, 1913–1988, *Pure appl. Geophys.*, **135**, 261–359.
- Yamamoto, Y. *et al.*, 2008. Spatial heterogeneity of the mantle wedge structure and interplate coupling in the NE Japan forearc region, *Geophys. Res. Lett.*, **35**, L23304, doi:10.1029/2008GL036100.
- Yoshii, T., 1979. A detailed cross-section of the deep seismic zone beneath northeastern Honshu, Japan, *Tectonophysics*, **55**, 349–360.
- Zhang, H. & Thurber, C.H., 2003. Double-difference tomography: the method and its application to the Hayward Fault, California, *Bull. seism. Soc. Am.*, **93**, 1875–1889.
- Zhao, D., Hasegawa, A. & Kanamori, H., 1994. Deep structure of Japan subduction zone as derived from local, regional and teleseismic events, *J. geophys. Res.*, **99**, 22 313–22 329.

SUPPORTING INFORMATION

Additional Supporting Information may be found in the online version of this paper:

Figure S1. Locations of six (c–h) recent earthquakes in the aftershock area of the 1933 earthquake. Earthquakes c–e occurred in the outer trench area and earthquakes f–h in the inner trench area. Earthquake a and b are the ones whose waveforms are shown in Fig. 2. Recent earthquakes were selected in the similar magnitude range as the 1933 aftershocks. The blue and orange circles are the same as those in Fig. 8(a).

Figure S2. Seismograms of the 1933 aftershocks (a, b) and recent earthquakes (c–h). The locations of the earthquakes are shown in Fig. S1. For the recent earthquakes, we simulated the record of the 1933 Oomori seismometer by convolving instrument

response assuming a period of 16 s and damping of 0.2. The period is from the Mizusawa catalogue and the damping constant is from visual inspection of waveforms because this constant was not documented. The records for the recent earthquakes are EW component recorded at Esashi station by an STS-2 broad-band seismometer.

Table S1. Relocated hypocentres using 3-D seismic wave speed and a double-difference relocation procedure, measured S – P times and dominant frequencies determined in this study. Solutions

with depths slightly above the earth's surface are set to zero depth.

(<http://gji.oxfordjournals.org/lookup/suppl/doi:10.1093/gji/ggw234/-/DC1>).

Please note: Oxford University Press is not responsible for the content or functionality of any supporting materials supplied by the authors. Any queries (other than missing material) should be directed to the corresponding author for the paper.